Excitation of Alfvén eigenmodes by low energy beam ions in the DIII-D and JET tokamaks[a)]

R. Nazikian,[1,b)] N. N. Gorelenkov,[1] B. Alper,[2] H. L. Berk,[3] D. Borba,[4] R. V. Budny,[1] G. Y. Fu,[1] W. W. Heidbrink,[5] G. J. Kramer,[1] M. A. Makowski,[6] S. D. Pinches,[2] S. E. Sharapov,[2] W. M. Solomon,[1] E. J. Strait,[7] R. B. White,[1] M. A. Van Zeeland,[7] and JET-EFDA contributors[c)]

[1]*Princeton Plasma Physics Laboratory, Princeton, New Jersey 08543, USA*
[2]*Euratom/UKAEA Fusion Association, Culham Science Centre, Abingdon OX14 3DB, United Kingdom*
[3]*University of Texas at Austin, Austin, Texas 78712, USA*
[4]*Euratom/IST Fusion Association, Centro de Fusao Nuclear, Lisboa, Portugal*
[5]*University of California Irvine, Irvine, California 92697, USA*
[6]*Lawrence Livermore National Laboratory, Livermore, California 94550, USA*
[7]*General Atomics, San Diego, California 92186-5608, USA*

(Received 13 November 2007; accepted 10 January 2008; published online 27 February 2008)

Core localized Alfvén eigenmodes in DIII-D [J. L. Luxon, Nucl. Fusion **42**, 614 (2002)] and Joint European Torus (JET) [P. H. Rebut and B. E. Keen, Fusion Technol. **11**, 13 (1987)] plasmas are driven by deuterium neutral beam ions traveling well below the Alfvén speed. Modes are observed in reverse magnetic shear discharges with deuterium ion velocities as low as 0.23 and 0.16 of the Alfvén speed parallel to the magnetic field in DIII-D and JET plasmas, respectively. Ellipticity-induced Alfvén eigenmodes in DIII-D and toroidicity-induced Alfvén eigenmodes in JET are excited by deuterium ions traveling well below the fundamental passing ion resonance condition, indicating the role of high-order resonances in driving these modes. NOVA-K analysis reveals many high-order resonances as contributing to the mode drive at high central safety factor due to the correspondingly large poloidal orbit width and the decrease in the perpendicular scale length of the modes. © *2008 American Institute of Physics*. [DOI: 10.1063/1.2839286]

I. INTRODUCTION

In a future burning plasma device such as ITER,[1] the partial pressure of alpha particles born from deuterium tritium reactions and other sources of suprathermal ions such as radio frequency heating and neutral beam injection (NBI), will form a significant fraction of the central plasma pressure. This is particularly the case in enhanced confinement steady-state regimes with reversed magnetic shear and elevated magnetic safety factor.[2] Simulating the collective effects of such a population of energetic ions in these advanced configurations is a major goal of the international fusion effort and several methods are used to attempt such simulations. Foremost among these is the radio frequency acceleration of deeply trapped minority ions in the MeV range of energy,[3–5] or the use of very high energy neutral atoms injected in the direction of the plasma current.[6] In these methods the interaction between energetic ions and plasma waves is principally through the precessional motion of deeply trapped ions or the transit motion of untrapped ions in the direction of the plasma current.

For low energy neutral beam ions ($E_b \leqslant 120$ keV) injected in the direction of the plasma current, it is generally assumed that the toroidal magnetic field must be sufficiently low in order to excite Alfvén instabilities, based on the fundamental passing particle resonance condition, where the beam ion velocity is typically a large fraction of the Alfvén velocity.[7–10] In particular, no significant effort has been invested in attempting to excite modes below the fundamental resonance condition for toroidal Alfvén eigenmodes[11] (TAEs), the ellipticity-induced Alfvén eigenmode[12] (EAE) or any other Alfvén eigenmode.

New results presented in this paper demonstrate clearly the excitation of Alfvén eigenmodes well below their fundamental resonance condition for passing ions. These results indicate the importance of multiple high-order resonances in the excitation of Alfvén eigenmodes and reveal that a large fraction of the fast ion population can be resonant with these modes when the central safety factor is high. Experimental observations of beam ion driven Alfvén eigenmodes at high toroidal field in DIII-D[13] and Joint European Torus[14] (JET) are presented in Sec. II. Profile analysis and NOVA calculations are used to identify the modes in Sec. III. Section IV presents the results of stability analysis for EAEs in DIII-D and TAEs in JET using the NOVA-K code to identify the role of high-order resonances in mode excitation. The implications of many high-order resonances on particle transport are discussed in the conclusion.

II. OBSERVATIONS

Figure 1 displays spectra of Alfvén eigenmode activity observed during neutral beam injection in the DIII-D tokamak. The modes are excited early in the discharge by deuterium atoms injected into the plasma in the direction of the

[a)]Paper JI1 1, Bull. Am. Phys. Soc. **52**, 140 (2007).
[b)]Invited speaker. Electronic mail: rnazikian@pppl.gov.
[c)]See Appendix of M. L. Watkins *et al.*, *Fusion Energy 2006*, Proceedings of the 21st International Conference, Chengdu, 2006 (IAEA, Vienna, 2006).

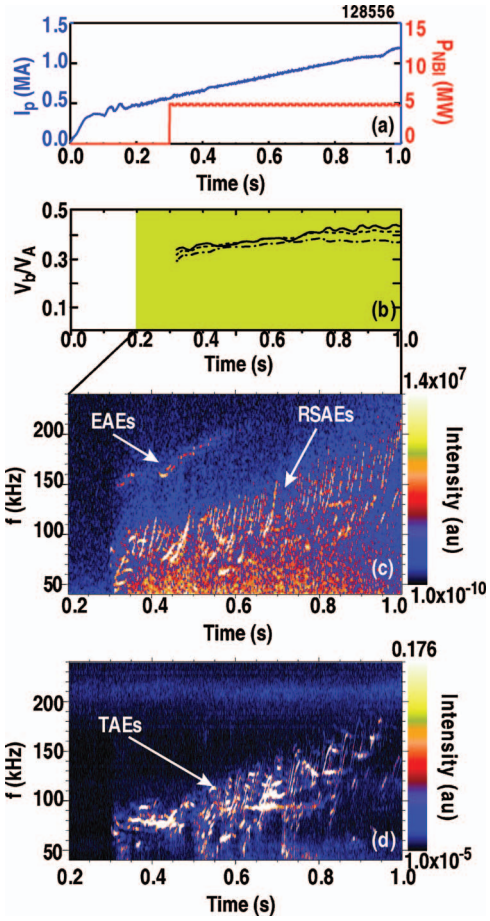

FIG. 1. (Color) Evolution of plasma parameters and Alfvén eigenmode activity in DIII-D discharge #128556. Shown are (a) evolution of plasma current I_P and neutral beam power P_{NBI}; (b) ratio of deuterium beam ion velocity V_b to Alfvén velocity V_{A} during the neutral beam injection phase for three normalized minor radii corresponding to $\rho=0.2,0.4,0.6$; (c) spectrum of density fluctuations taken with the radial midplane CO_2 laser interferometer; and (d) the spectrum of magnetic fluctuations received on magnetic pickup loops at the vacuum vessel wall on the outer midplane. Plasma parameters at $t=0.5$ s are $B_T=2.0$ T, $I_p=0.8$ MA, $n_e(0)=2.3\times10^{13}$ cm^{-3}, $T_e(0)=1.8$ keV, $T_i(0)=2.1$ keV, and $q_{\min}\simeq3.5$.

toroidal current. These atoms ionize in the plasma core with an initial pitch angle $V_{\parallel}/V_b\simeq0.65$, corresponding to $\chi=V_{\perp}/V_b\simeq0.75$ and energy $E_b\simeq75$ keV, where V_b is the particle speed and $V_{\parallel}$ is the velocity parallel to the magnetic field line. The mode activity is most intense in the initial phase of the discharge when the minimum magnetic safety factor is highest ($q_{\min}>3$). The distribution of the beam ions in both pitch angle and energy is expected to spread due to Coulomb collisions and this spreading is calculated using the TRANSP code.[15]

The dominant Alfvénic modes driven by neutral beam ions in DIII-D are the reverse shear Alfvén eigenmodes (RSAEs, also known as Alfvén cascades) and toroidal Alfvén eigenmodes (TAEs).[16–18] The properties of these modes in DIII-D (frequency, radial structure, magnitude) have been well documented in recent years.[19–21] For the present study, we focus on the observation of higher frequency ellipticity-induced Alfvén eigenmodes (EAEs) because these modes typically require higher fast ion velocities for their excitation relative to the RSAE and the TAE. The spectra of CO_2 laser interferometer data[22] in Fig. 1(c) reveals modes in the EAE frequency range very early in the discharge and these modes persist for only 0.3 s before disappearing. The EAE is expected to occur at about twice the TAE frequency. The EAE is also observed on electron cyclotron emission measurements from the plasma core. From Fig. 1, at $t=0.4$ s the TAE frequencies occur in the range 75–95 kHz [Fig. 1(d)], whereas the EAE frequency is close to 160 kHz [Fig. 1(c)].

The EAEs are observed on the central electron cyclotron emission (ECE) channels in the region $r/a=0.2$–0.4 and are not observed on the magnetic sensors [Fig. 1(d)], indicating that they are highly core localized. The magnetic sensors are sensitive to poloidal magnetic oscillations at the plasma edge. Modes that do not extend to the edge of the plasma will not be observed on the magnetic sensors, even if they are of large amplitude in the plasma core. Another example that highlights the different sensitivity of the interferometer and magnetic sensors is for the RSAE and TAE. In Fig. 1(d) we can observe very strong magnetic signals associated with TAE modes that are not well observed on the interferometer chord in Fig. 1(c). From the external magnetic measurements, the toroidal mode numbers for the TAEs are in the range $n=2$–5. Conversely, the RSAEs (rapid frequency chirping modes) are well observed on the interferometer signal [Fig. 1(c)] but are not particularly strong on the magnetic sensors. Nonetheless, the magnetic sensors reveal low-n modes corresponding to the most radially extended RSAEs.[20]

At the highest operating toroidal field, the 75 keV deuterium beam ions travel near 0.35 of the Alfvén velocity (V_{A}), while the component of the ion motion in the direction of the magnetic field corresponds to $V_{\parallel}/V_b\simeq0.23$. For the experiments discussed in this paper, only the tangential beams were employed. However, even for the tangential beams the pitch angle to the magnetic field lines is significant in the plasma core as noted above. This is also similar for the JET tangential beams. Coulomb collision will spread the pitch angle distribution to some extent, particularly at low energies; however, the dominant component of the distribution at the injection energy will be at or near the injection pitch angle.

From Fig. 1(b), the ratio of the beam ion to Alfvén velocity in the early phase of the discharge is $\simeq0.35$, corresponding to $V_{\parallel}/V_{\mathrm{A}}\simeq0.23$ in the interval between 0.3 and 0.6 s, for a range of normalized minor radii ($\rho=0.2,0.4,0.6$) spanning the region where the core localized mode activity is expected to occur. This is well below the usual resonance condition for passing particle excitation of EAEs, given by $V_{\parallel}=\pm0.5V_{\mathrm{A}}$. To understand how excitation can occur below the fundamental resonance condition, we introduce a general expression for wave-particle resonance given by

$$\omega=[(m-nq)+p]\omega_\theta+n\omega_{\mathrm{pr}}, \tag{1}$$

where $\omega_\theta=V_{\parallel}/qR$ is the poloidal particle transit frequency, ω is the mode frequency in the plasma frame, ω_{pr} is the particle toroidal precession frequency, m and n are the poloidal and toroidal mode numbers, respectively, q is the magnetic safety factor, R is the major radius, and p is a nonzero integer. For deeply trapped ions, the resonance condition is determined

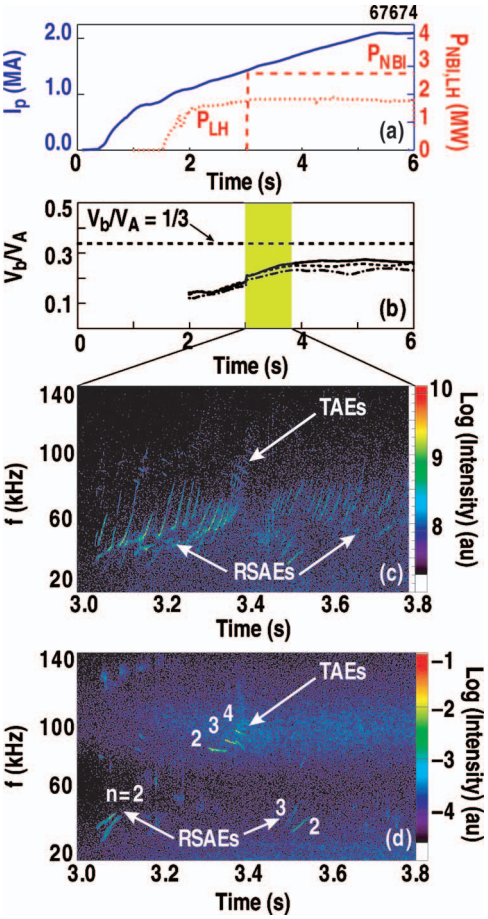

FIG. 2. (Color) Evolution of plasma parameters and Alfvén eigenmode activity in JET discharge #67674. Shown are (a) evolution of plasma current I_p, lower hybrid power P_{LH}, 115 keV deuterium neutral beam power P_{NBI}; (b) ratio of deuterium beam ion velocity V_b to Alfvén velocity V_A for three normalized minor radii $\rho=0.2,0.4,0.6$; (c) spectrum of density fluctuations taken with the radial midplane O-mode interferometer; and (d) the spectrum of magnetic fluctuations received on magnetic pickup loops at the vacuum vessel wall on the outer midplane. Plasma parameters at $t=3.4$ s are $B_T=3.45$ T, $I_p=1.5$ MA, $n_e(0)=1.3\times10^{13}$ cm^{-3}, $T_e(0)=6.3$ keV, $T_i(0)=1.9$ keV, and $q_{\min}\simeq3.5$.

by the precession frequency $\omega\simeq n\omega_{pr}$, whereas for passing ions the primary contribution is from the poloidal transit frequency.

The fundamental passing particle resonance condition ($p=\pm1$) represents the strongest channel of wave-particle interaction when $k_\perp\rho_b\ll1$, where $k_\perp\simeq nq/r$ is the perpendicular wavenumber of the mode, r is the minor radius, and ρ_b is the beam ion Larmor radius. For EAEs, $m-nq=\pm1$ and $\omega\simeq V_A/qR$, so that the fundamental particle resonance condition is given by $V_\parallel\simeq\pm0.5V_A$.[23] In this limit of $k_\perp\rho_b$, the drive from fast ions drops off dramatically once the injection velocity falls below $0.5V_A$. However, for $k_\perp\rho_b\sim1$ we expect many higher-order resonances to play a role, leading to a significant reduction in the resonant velocity for interaction with the modes. We return to this point when discussing the stability analysis in Sec. IV.

Figure 2 shows a similar discharge obtained on the JET tokamak for beam driven TAEs excited below the fundamental resonance condition. A key difference between the JET and DIII-D experiments is the use of lower hybrid current drive in JET for raising the central safety factor in the core and creating strongly reversed magnetic shear discharges for the investigation of advanced confinement and steady-state regimes.[24] The dominant modes in JET are the RSAEs; however, weaker higher frequency modes in the TAE range of frequency are observed with deuterium beam ion injection. One difference between the JET and DIII-D experiments is that JET neutral beams typically operate in the range $E_b=115-140$ keV. The deuterium beams are injected in the direction of the plasma current, as in the DIII-D experiments. In a systematic scan of the beam injection energy, TAEs were observed for E_b as low as 115 keV in a 3.45 T discharge corresponding to $V_b\simeq0.25V_A$ at the time of interest ($t=3.4$ s), as shown in Fig. 2(b). This corresponds to $V_\parallel/V_A\simeq0.16$. This is well below the fundamental resonance condition $V_\parallel=1/3V_A$.[25] Figure 2(c) shows the spectrogram of density fluctuations taken using an O-mode reflectometer system that operates as a radial midplane interferometer for reflection from the back wall of the vacuum vessel.[4] Activity in the TAE and RSAE range of frequency is simultaneously observed on external magnetic sensors [Fig. 2(d)], where mode number identification is possible, at least for the lowest toroidal mode numbers ($n=2-5$) corresponding to the most radially extended modes.

III. NOVA ANALYSIS

The NOVA code[26] is used to identify the EAE and TAE modes and their radial structure based on the available experimental data from DIII-D and JET, respectively. Figure 3(a) shows a high resolution plot of the interferometer spectrum in Fig. 1(c) during the period of EAE activity. Also shown is the evolution of the EAE frequency $f_{EAE}=V_A/2\pi qR$, based on the evolution of the plasma density and magnetic safety factor at $\rho=0.4$. This location for the estimate of the EAE frequency is based on the NOVA analysis of the mode location, shown in Fig. 3(b). The NOVA analysis for the EAEs is performed at $t=0.5$ s. At this time, the plasma q-profile is indicated in Fig. 3(b) with $q_{\min}\simeq3.5$ from motional Stark effect (MSE) measurements.[27]

The radial displacement for three eigenmodes in the ellipticity induced gap in the shear Alfvén spectrum are shown in Fig. 3(b) corresponding to three different toroidal mode numbers: $n=3,4,5$. The absence of magnetic fluctuations outside the plasma prevents a definitive identification of the mode numbers. The observed frequency separation in the data is about 7 kHz, which is very close to the separation of frequencies in the NOVA analysis and is also close to the charge exchange recombination spectroscopy[28] measurement of the impurity rotation in these plasmas. The strong central peaking of the eigenmodes confirms the absence of magnetic fluctuations at the plasma boundary.

The NOVA solutions for the EAEs possess several poloidal mode harmonics, but the dominant modes are two poloidal harmonics m and $m+2$, which couple through the plasma elongation, where $m\simeq nq$. For $q_{\min}\simeq3.5$, we expect very high poloidal mode numbers in the range $m=11-18$ for $n=3-5$, consistent with the range calculated by NOVA. For a 75 keV injected beam ion with Larmor radius $\rho_b\simeq2.0$ cm

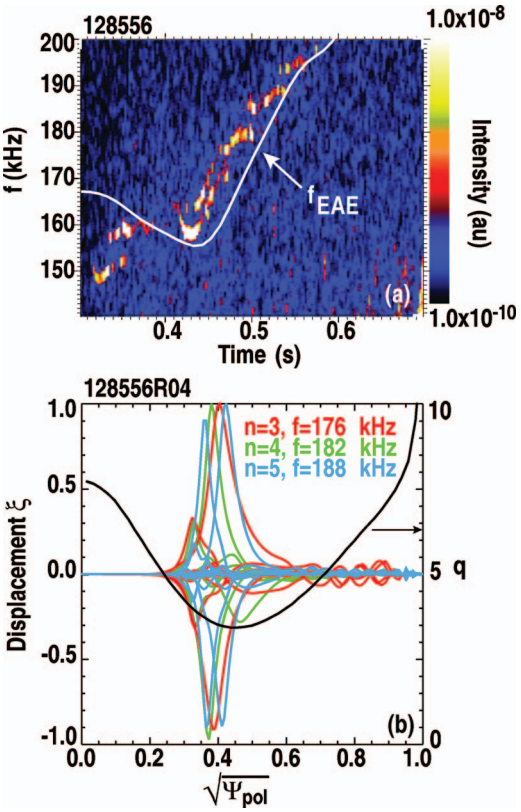

FIG. 3. (Color) Evolution in DIII-D of (a) EAE density fluctuations from CO_2 laser interferometer measurements overlayed with the expected EAE frequency calculated near $\rho=0.4$ and (b) normalized radial displacement for $n=3,4,5$ EAEs calculated using the NOVA code for the equilibrium profile taken at $t=0.5$ s with q-profile shown. The mode displacement for each toroidal mode number and for a range of poloidal mode numbers are shown in red ($n=3$), green ($n=4$), and blue ($n=5$) vs poloidal flux coordinates $\psi_{\rm pol}^{1/2}$.

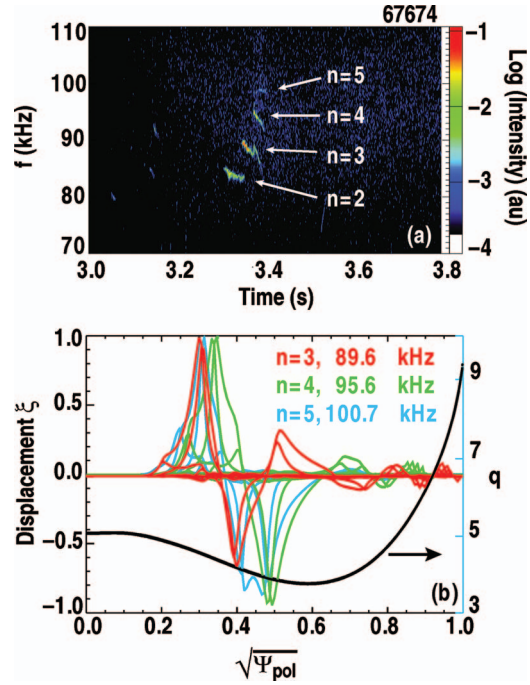

FIG. 4. (Color) Evolution in JET of (a) TAE edge magnetic fluctuations overlayed with the measured toroidal mode numbers and (b) normalized radial displacement for $n=3,4,5$ TAEs calculated using the NOVA code for the equilibrium profile taken at $t=3.4$ s with q-profile shown. The mode displacement for each toroidal mode number and for a range of poloidal mode numbers are shown in red ($n=3$), green ($n=4$), and blue ($n=5$) vs poloidal flux coordinates $\psi_{\rm pol}^{1/2}$.

and minor radius $r\simeq 20$ cm, we have $k_\perp\rho_b\simeq 1-2$, well in the range where higher-order resonance $|p|>1$ can significantly contribute to the mode drive.

The NOVA code[26] is also used to identify TAEs in JET. Figure 4(a) shows a higher resolution plot of the magnetic spectra in Fig. 2 during the period of TAE activity around $t=3.4$ s. The TAE frequency, i.e., $f_{\rm TAE}=V_{\rm A}/4\pi qR$, is close to the observed frequency range near $\rho=0.4$ for $q_{\rm min}\simeq 3.5$, obtained from MSE measurements. The location of the TAEs, inferred from NOVA, are in the range $\rho=0.2-0.6$, shown in Fig. 4(b). Unlike the case for EAEs in DIII-D, the TAEs in JET are detected on both the interferometer and magnetic diagnostics, allowing for a definitive identification of their toroidal mode number. From Fig. 4(a), the dominant toroidal mode numbers are in the range $n=2-4$ with a frequency separation $\simeq 6$ kHz. The NOVA analysis in Fig. 4(b) agrees closely with the measured mode frequencies for the same range of toroidal mode numbers and accurately recovers the frequency separation between the modes due to toroidal rotation.

The NOVA solutions for the TAEs also possess several poloidal mode harmonics but the dominant modes are two poloidal harmonics m and $m+1$, which couple through the plasma toroidicity, where again $m\simeq nq$. For $q_{\rm min}\simeq 3.5$ we again expect very high poloidal mode numbers in JET as with DIII-D, in the range $m=11-18$ for $n=3-5$, consistent with the range calculated by NOVA. However, the size of the plasma and the toroidal magnetic field strength are both higher in JET, so that $k_\perp\rho_b$ is expected to be lower. For $E_b=115$ keV, $B_T=3.45$ T and $r\simeq 40$ cm at the mode location we obtain $k_\perp\rho_b\simeq 0.4-0.8$.

IV. STABILITY ANALYSIS

The stability of EAEs in DIII-D and TAEs in JET are studied using the linear stability code NOVA-K, which takes into account the realistic beam ion distribution including beam anisotropy, collisional broadening, and the slowing down distribution.[29] This code uses the ideal magnetohydrodynamic (MHD) solutions generated by NOVA and calculates the drive and damping using a perturbative procedure incorporating the fast ion distribution based on TRANSP analysis[30] in addition to various damping terms such as ion and electron Landau damping. The NOVA analysis reveals that the mode drive is more than sufficient to overcome the damping for these core localized modes in DIII-D and JET, consistent with our observations. However, until recently, the NOVA-K code has not been used to resolve the dominant order of the resonant interaction responsible for mode excitation. Such resonance investigations have been carried out on JET using the HAGIS code for deeply trapped minority ions.[31] The experiments performed with co-injected neutral beam ions in JET and DIII-D that are described in this paper makes clear that the fundamental resonance condition is not satisfied for passing ions so the NOVA-K code has recently been modified

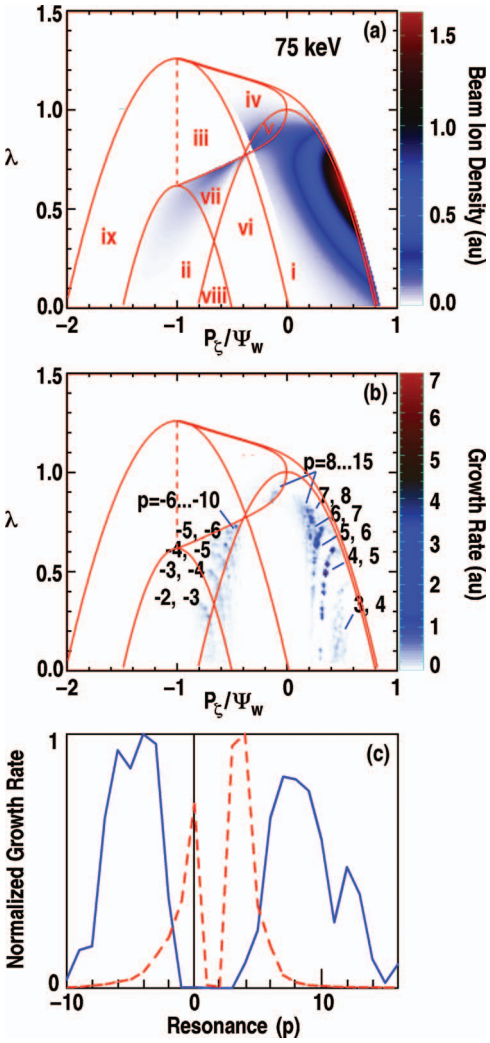

FIG. 5. (Color) Contribution of beam ion distribution to the linear growth rate for an $n=4$ EAE in DIII-D calculated using the NOVA-K code. (a) Contours of the beam ion distribution at 75 keV vs pitch angle variable $\lambda=\chi^2 B_0/B$, $\chi=V_\perp/V_b$ and normalized canonical momentum P_ζ/ψ_W with trapped passing particle boundaries for 75 keV ions indicated by the red curves. The particle orbit regions correspond to co-passing ions (i), counter-passing ions (ii), trapped lost ions (iii), trapped confined ions (iv), potato orbits (v), co-lost orbits (vi), a mixture of counter-passing and co-lost orbits (vii), co-lost and counter-confined orbits (viii), and counter-lost orbits in (ix). The beam ions are injected into the co-passing region with large perpendicular energy. (b) Contours of linear growth rate on the same coordinates. The dominant contribution to the mode drive comes from the co-going orbits, with significant additional contribution from counter-going particles in region (vii) from scattered ions. (c) The total contribution to the linear growth rate is shown for each resonance p for the case of deuterium (blue) and for an artificial particle with the same deuterium beam ion distribution and mass but with charge $z=100$ (dashed red line) in order to remove finite orbit width and precessional effects. The value of p is estimated by assuming $m\simeq nq$ in NOVA-K, valid for modes with high $nq_{\min}$. The peak contribution to the drive clearly shifts to high-order resonances when finite orbit effects are included.

to include additional diagnostics in order to resolve the relevant resonant interactions.

Figure 5(a) displays a plot of the analytical beam ion distribution generated for 75 keV beam ions at the time of interest for the plasma in Fig. 1 (see Ref. 29) together with the boundaries representing different classes of orbits. The contours represent beam ion density plotted in terms of normalized fast ion invariants of the motion $\lambda=\chi^2 B_0/B \simeq \chi^2 R/R_0$ and P_ζ/ψ_W, where $\chi=V_\perp/V_b$ is the pitch angle, $P_\zeta=V_\parallel B_0/B-\psi_{\rm pol}(r)$ is the canonical momentum, $\psi_{\rm pol}(r)$ is the usual poloidal magnetic flux at minor radius r, ψ_W is the poloidal flux at the last closed flux surface, B is the local magnetic field strength, B_0 is the magnetic field strength on the magnetic axis.[32] The advantage of this representation is that it readily identifies the class of particle orbits (deeply trapped, co- or counter-passing, potato or stagnation, nearly trapped, etc.) that make up the distribution of the ions at a given energy. Most of the beam ions are deposited in a small region of phase space for co-moving ions with weak collisional broadening into other orbit classes.

From an experimentalist's perspective, the map in Fig. 5(a) can be interpreted as follows. Moving up the vertical axis, the pitch angle (χ) of the particle relative to the magnetic field line increases so particles are deeply passing at low values of the vertical axis (λ) and deeply trapped at the upper range. Along the horizontal axis, particles are moving in the direction counter to the plasma current to the far left and move in the direction of the plasma current toward the right, with an offset determined by the magnetic flux at the particle location. The regions of passing and trapped orbits are indicated in Fig. 5(a) by the red lines for 75 keV deuterium ions; however, these boundaries do not change significantly over a wide range of energies. Region (i) corresponds to passing particles traveling in the direction of the plasma current and the right hand side of this region represent well confined passing ion orbits. A small fraction of the ions at 75 keV are scattered into trapped confined orbits (region iv), potato orbits (v), and counter-passing orbits (ii). Region (iii) represents lost trapped orbits and region (vii) represents a mixture of lost co-going and confined counter-going orbits.

Figure 5(b) displays a map of all the relevant contributions of fast ions to the $n=4$ EAE mode drive in DIII-D together with the boundaries representing the different classes of orbits as in Fig. 5(a). The color contours represent the strength of contribution to the EAE mode drive from a particular region of the fast ion distribution including all particle energies, plotted against the normalized fast ion invariants of the motion. The advantage of this representation is that it readily identifies the class of particle orbits (deeply trapped, co- or counter-passing, potato or stagnation, nearly trapped, etc.) that contribute most strongly to the mode drive. The figure clearly shows bands of contribution to the mode drive and each of these bands corresponds to a particular combination of high-order resonances represented by the parameter p in Eq. (1). The large perpendicular energy of the resonant particles in Fig. 5(a) confirms the large value of $k_\perp \rho_b \simeq 1-2$ attributed to these modes.

Figure 5(b) shows a strong contribution to the mode drive coming from the region where 75 keV beam ions are injected into the plasma [Fig. 5(a)]. The distribution broadens and spreads at lower energies, accounting for the contribution to the mode drive at pitch angles away from the injected value. In addition, there is a surprisingly strong resonant contribution from counter-passing confined ions with large pitch angles. This is clear from the fact that in regions (ii) and (vii) there are strong bands of contribution to

the mode drive. It is instructive to observe that there is almost no contribution from trapped confined ions that exhibit the usual banana orbits (region iv); however, there is a contribution to the drive from the trapped potato orbits (region v). Region (iii) represent lost trapped orbits, so it is comforting that no drive is computed to arise from this region. Just below region (iii) there is a dense band of resonances consisting of counter-going confined orbits that is very close to the counter-passing trapped lost orbit boundary (iii). The fact that the counter-going orbits in (vii) are so close to the loss boundary (iii) suggests that perturbations of the particle orbits in this region could readily lead to large losses.

Passing orbits with large pitch angle to the magnetic field, and hence low velocity along the magnetic field, can only interact with the mode through high-order resonances and this is in fact revealed by the NOVA-K analysis. Figure 5(b) shows for each resonance band the order of the wave-particle resonances p that contributes most to the drive. The dominant resonance clearly shifts to higher orders as the pitch angle increases, consistent with a reduction in the parallel velocity of the ions with increasing pitch angle. To better understand the structure of the resonances in Fig. 5(b), we refer to Eq. (1), and for simplicity ignore the role of precession. Assuming $\omega = k_\parallel V_A$ and $k_\parallel = 1/lqR$ for shear Alfvén waves, we obtain

$$\frac{V_\parallel}{V_b} = \left(\frac{V_A}{V_b}\right)\frac{1}{lp \pm 1}, \tag{2}$$

and for $\chi = V_\perp / V_b$, then

$$\chi^2 = 1 - \left(\frac{V_A}{V_b}\right)^2 \frac{1}{(lp \pm 1)^2} \geqslant 0, \tag{3}$$

where V_b is the beam ion velocity. In the following we note that χ^2 is qualitatively similar to λ and $V_\parallel / V_b$ is qualitatively similar to P_ζ / ψ_W. From Eq. (3), as p increases, the pitch angle χ rapidly approaches unity for constant particle energy. This can be understood by noting that from Eq. (2), $V_\parallel$ must decrease as the order of the resonance increases for constant V_b in order to maintain resonance. A consequence is that the particle pitch angle must increase as p increases. Note that the red boundary curve on the right of region (i) denotes orbits of constant energy (75 keV). As λ increases along this curve, the dominant order of the resonance p also increases until the resonances blur together at large pitch angle. This same accumulation of high-order resonances at large λ occurs for negative $V_\parallel / V_b$, but in this case the dominant resonant orders are negative, not positive. This can be understood by noting from Eq. (2) that p must reverse sign when $V_\parallel / V_b$ reverses sign in order to maintain resonance.

For a given p, then we obtain a range of energies that can satisfy the resonance condition, each with a different χ, marking out the resonant arcs seen in Fig. 5(a). For a given value of p corresponding to one of the arcs in Fig. 5(b), then from Eq. (3), the pitch angle increases toward unity with increasing energy. This is again a simple consequence of Eq. (2), where $V_\parallel$ is constant for a given p and thus the pitch angle must increase with energy in order to maintain the resonance. Detailed analysis of the NOVA-K output confirms this prediction.

One outstanding question is why there is a strong contribution from high-order resonances ($p > 5$) in the first place, as the coupling to higher-order resonance is expected to be weak. The blue curve in Fig. 5(c) shows the total integrated contribution to the linear growth rate for each resonance. The figure clearly shows that the peak contribution is from $p = -4, +7$. It is likely that the dominance of the higher order resonances is due to finite orbit width effects.[33] In order to test this hypothesis, we repeated the stability analysis using ions with the same mass and velocity distribution as the deuterium but with charge $Z = 100$ for the particle electric charge. The net effect of this charge increase is to dramatically reduce the particle orbit width. The result is shown by the red dashed curve in Fig. 5(c). Unlike the original case where full orbit effects are included, the dominant resonance moves down to $p = 3, 4$ with a rapid falloff at higher orders, as is expected for cases where $k_\perp \rho_b \ll 1$. The dominant resonance for this case corresponds to the lowest-order deeply passing ion resonance accessible to the beam ions, confirming the role of finite orbit effects in shifting the dominant resonance to higher orders.

Figure 6 shows a similar example calculated for JET for the $n = 4$ TAE in Fig. 4(b). The distribution and spread of 115 keV beam ions in Fig. 6(a) is very similar to the DIII-D case in Fig. 5(a). The principal difference between the JET case for the TAE and the DIII-D case for the EAE is that in JET, NOVA-K computes a dominant interaction through only two high-order resonances corresponding to $p = 4, 5$, which provides $\simeq 10\times$ greater contribution to the drive than the next strongest resonance. For this reason the contour plot in Fig. 6(b) is shown in log scale, unlike the linear scale in Fig. 5(b). Injected beam ions in JET have a similar pitch angle to DIII-D, so from the above argument, the parallel velocity is close to $V_\parallel / V_A \simeq 0.16$ at the time of interest, $t = 3.4$ s. From Fig. 6(a) we observe that the dominant contribution to the drive comes from high-order resonances close to the injected pitch angle. The lowest accessible resonance for the beam ions is $p = 3$; however, this is not the dominant contribution to the drive. The phase space distribution of the resonant particles contributing to the drive and the sequence of increasing high-order resonances with increasing λ are qualitatively similar to the case of DIII-D, indicating that the basic mechanism of mode excitation is the same. Namely, the dominant contribution to the drive comes from passing beam ions with relatively high pitch angle.

It is striking that the contribution of higher-order resonances to the TAE drive in JET [Fig. 6(c)] is similar to the resonance contribution from beam ions to the EAE drive in DIII-D [Fig. 5(c)] in the case where the orbit width was reduced by increasing the particle charge. This leads us to suspect that the orbit width effect in beam ion excitation of Alfvén eigenmodes in DIII-D is considerably stronger than in high field JET plasmas for tangentially injected beam ions. An interesting distinction between the JET and DIII-D beam ion orbits is that in JET the orbit width effect is expected to be smaller than in DIII-D due to the higher toroidal field and larger scale. For a larger plasma, we expect $k_\perp \simeq nq/r$ to

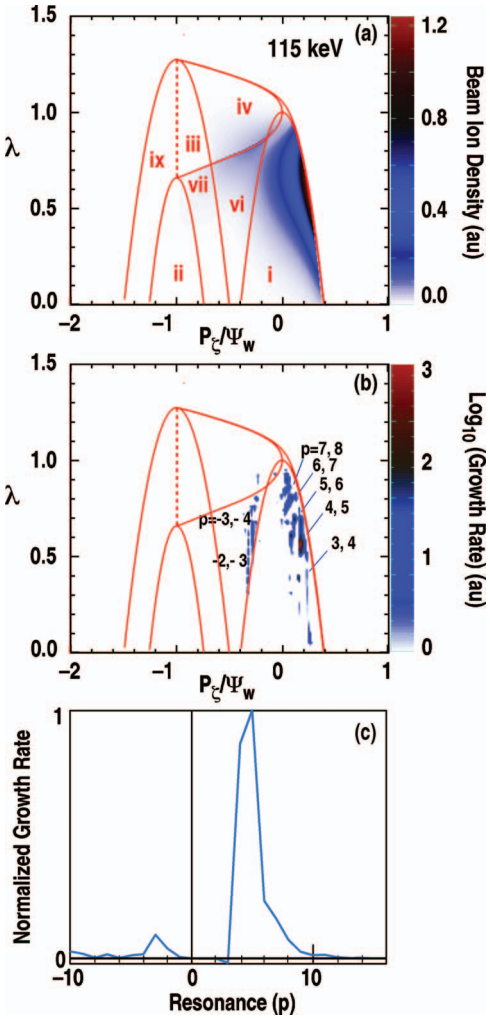

FIG. 6. (Color) Contribution of beam ion distribution to the linear growth rate for an $n=4$ TAE in JET calculated using the NOVA-K code. (a) Contours of the beam ion distribution at 115 keV vs pitch angle variable $\lambda=\chi^2 B_0/B$ and normalized canonical momentum P_ζ/ψ_W with trapped passing particle boundaries for 115 keV ions indicated by the red curves, as in Fig. 5(a). (b) Contours of linear growth rate on the same coordinates. The dominant contribution to the mode drive comes from the co-going orbits, with significant additional contribution from counter-going particles in region (vi) from scattered ions. (c) The total contribution to the linear growth rate is shown for each resonance p. The value of p is estimated by assuming $m \simeq nq$ in NOVA-K, valid for modes with high $nq_{\min}$.

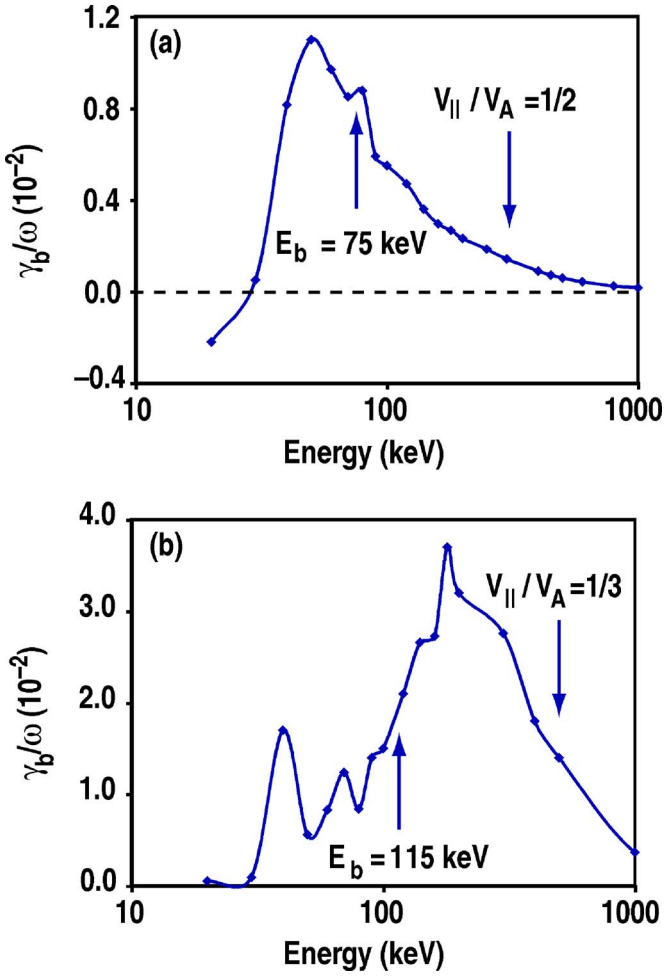

FIG. 7. (Color online) Linear beam ion drive (γ_b/ω) computed using NOVA-K vs beam injection energy for the $n=4$ EAE in DIII-D (a) and the $n=4$ TAE in JET (b) for modes shown in Figs. 3(b) and 4(b), respectively. The deuterium beam injection energy is scanned keeping the fast ion pressure constant. The energy corresponding to the fundamental resonance for passing ions [$V_{||}/V_A=1/2$ for EAEs in (a) and 1/3 for TAEs in (b)] are indicated by the vertical arrows. Total mode damping in both cases is dominated by collision electron damping and is of the order 0.1%, or roughly 10% of the peak beam ion drive.

decrease for the same q, n. In addition, the higher toroidal field will decrease ρ_b, with some modest increase from the higher beam ion energy (115 keV in JET versus 75 keV in DIII-D). The reduction in $k_\perp \rho_b$ from 1–2 in DIII-D to 0.4–0.8 in JET for these plasmas may be sufficient to account for the reduced range and number of resonances in the NOVA-K analysis for TAEs on JET.

Note that for large p we have for the resonance condition $V_{||} \simeq \omega qR/p$ for passing ions, where ω is the mode frequency. This is instructive because it points to a qualitative change in the resonance properties of waves at high and low orders. For a given high-order p, and for gap modes $\omega=V_A/lqR$, where l is an integer, the resonant parallel velocity of passing ions simply scales as $V_{||}=V_A/lp$. For TAEs $l=2$ and for EAEs $l=1$, so the resonant parallel velocity simply differs by a factor of two between the two modes. More generally, for a given q, the resonant $V_{||}$ scales linearly with the mode frequency at high p.

The ultimate effect of these high-order resonances is to destabilize Alfvén eigenmodes for beam injection energies well below those corresponding to the fundamental resonance condition. The calculated mode drive versus beam ion injection energy is evaluated using the NOVA-K code for the case of the $n=4$ EAE in DIII-D [Fig. 7(a)] and the $n=4$ TAE in JET [Fig. 7(b)]. In both cases, the energy corresponding to the fundamental resonance and the beam injection energy are indicated by the vertical arrows. In both DIII-D and JET the fast ion drive (γ_b/ω) is calculated to be large (of order 1%–2%). Indeed, for the EAE in DIII-D the mode drive is calculated to peak near the 75 keV and reduction of the beam energy to 50 keV (at constant fast ion beta) is only expected to increase the mode drive. In JET the mode drive appears to be decreasing with decreasing beam injection energy in the range 50–140 keV. In fact, carefully controlled experiments on JET indicate that reducing the beam ion energy from

115 to 80 keV, while maintaining similar discharge condition and fast ion beta, yields no observable TAEs. Calculation of the mode damping rate (γ_d/ω) in DIII-D and JET using NOVA-K code yields negligible ion Landau damping and dominant electron collision damping[34] of the order 0.1%, or roughly 10% of the calculated beam ion drive. These calculations are consistent with the observation of Alfvén eigenmodes driven by beam ions traveling well below the Alfvén velocity in both JET and DIII-D.

V. CONCLUSION

Deuterium neutral beam injection into high magnetic field DIII-D and JET discharges reveal the excitation of EAEs and TAEs with beam ion velocities well below the fundamental resonance condition for passing ions. Both TAEs in JET and EAEs in DIII-D are core localized based on the observed mode features and comparison to ideal MHD NOVA analysis. NOVA-K calculations of the mode stability based on TRANSP analysis of the beam ion distribution reveals strong mode drive coming from passing ion orbits with pitch angles larger than the injection angle. Analysis was performed using an artificially high deuterium charge in order to reduce the precession and orbit width effects. This had the effect of shifting the peak contribution to the lowest order accessible resonances with smaller pitch angles. This reveals the key role of finite orbit width in shifting the peak drive to high-order resonances.

An interesting observation is that large drive arises from beam ions scattered into counter-going orbits. These orbits are relatively fragile in that they are very close to loss boundaries. It is hypothesized that these counter-passing orbit particles may readily be removed from the plasma by interaction with instabilities or other nonuniform fields. An important test of the validity of these resonance calculations would be to look for particle losses at larger pitch angles than those injected into the plasma. Enhanced beam ion loss at large pitch angle during significant Alfvénic activity would indicate the importance of higher-order resonances in the excitation of these modes by toroidally injected beam ions.

A key outstanding question is what the dominant resonant interactions are expected to be for isotropic alpha particles and anisotropic beam ions in advanced steady state operating regimes in ITER. The peak drive for alpha particle driven instabilities in ITER is expected to be in the range $k_\perp \rho_\alpha \simeq 1$ for passing ions. This is similar to $k_\perp \rho_b$ in DIII-D for beam ions. The dominant drive in ITER is expected to be through the passing particle resonance, as with the modes observed in JET and DIII-D. However, a significant distinction is that the fundamental resonance condition is expected to be satisfied in ITER, corresponding to $V_\alpha/V_A \simeq 1$ for TAEs and 0.5 for EAEs. A key question for future analysis is whether the higher-order resonances will play a significant role in the excitation of Alfvén eigenmodes in burning plasmas even when the fundamental resonance is satisfied. Future studies will focus on the dominant resonant interactions for beam ions injected into DIII-D and JET with initial velocities that clearly satisfy the fundamental resonance condition, such as for RSAEs and TAEs in DIII-D shown in Fig. 1.

As a final point, it seems that the understanding of the nonlinear interaction between ideal MHD modes and fast ions must first start with a thorough analysis of all the relevant resonant interactions. Subtle issues affecting fast ion transport may arise according to whether one dominant low-order resonance or many high-order resonances are involved in the linear mode drive. In the future, more detailed analysis of the full range of resonant interactions between fast ions and Alfvén eigenmodes needs to be performed experimentally and theoretically.

ACKNOWLEDGMENTS

This work is partly supported by the U.S. Department of Energy under Contract Nos. DE-AC02-76CH03073, DE-FG03-97ER54415, SC-G903402, DE-FG03-01ER5461, DE-FG03-96ER54373, W-7405-ENG-48, and DE-FC02-04ER54698. The work is also partly performed under the European Fusion Development Agreement and is partly funded by Euratom and the UK Engineering and Physical Sciences Research Council. The authors would like to thank their colleagues at JET and DIII-D who operated the tokamaks, the heating systems, and the diagnostics during these experiments.

[1] K. Ikeda, Nucl. Fusion **47**, 1 (2007).
[2] T. C. Luce and DIII-D Team, Nucl. Fusion **45**, S86 (2005).
[3] H. Kimura, Y. Kusama, M. Saigusa *et al.*, Nucl. Fusion **38**, 1303 (1998).
[4] S. E. Sharapov, B. Alper, and J. Fessey, Phys. Rev. Lett. **93**, 016501 (2004).
[5] S. Bernabei, M. G. Bell, R. V. Budny *et al.*, Phys. Rev. Lett. **84**, 1212 (2000).
[6] Y. Kusama, G. J. Kramer, H. Kimura *et al.*, Nucl. Fusion **39**, 1837 (1999).
[7] D. Borba, B. Alper, R. V. Budny *et al.*, Nucl. Fusion **40**, 775 (2000).
[8] K. L. Wong, R. J. Fonck, S. F. Paul *et al.*, Phys. Rev. Lett. **66**, 1874 (1991).
[9] W. W. Heidbrink, E. J. Strait, E. J. Doyle *et al.*, Nucl. Fusion **31**, 1635 (1991).
[10] A. D. Turnbull, E. J. Strait, W. W. Heidbrink *et al.*, Phys. Fluids B **5**, 2546 (1993).
[11] C. Z. Cheng, L. Chen, and C. S. Chance, Ann. Phys. **161**, 1 (1985).
[12] R. Betti and J. P. Freidberg, Phys. Fluids B **3**, 1865 (1991).
[13] J. L. Luxon, Nucl. Fusion **42**, 614 (2002).
[14] P. H. Rebut and B. E. Keen, Fusion Technol. **11**, 13 (1987).
[15] R. J. Goldston, D. C. McCune, H. H. Towner *et al.*, J. Comput. Phys. **43**, 61 (1981).
[16] R. Nazikian, B. Alper, H. L. Berk *et al.*, *Proceedings of 20th International Atomic Energy Agency Fusion Energy*, Vilamoura, 2004 (IAEA, Vienna, 2005), www-pub.iaea.org/mtcd/meetings/PDFplus/fusion-20-preprints/index.htm, EX5-1.pdf.
[17] D. Borba, R. Nazikian, B. Alper *et al.*, *Proceedings of 21st International Atomic Energy Agency Fusion Energy*, Chengdu, 2006 (IAEA, Vienna, 2007), http://www-pub.iaea.org/MTCD/Meetings/fec2006presentations/PD-1.ppt.
[18] S. E. Sharapov, B. Alper, Yu. F. Baranov *et al.*, Nucl. Fusion **46**, S868 (2006).
[19] R. Nazikian, H. L. Berk, R. V. Budny *et al.*, Phys. Rev. Lett. **96**, 105006 (2006).
[20] M. A. Van Zeeland, G. J. Kramer, M. E. Austin *et al.*, Phys. Rev. Lett. **97**, 135001 (2006).
[21] G. J. Kramer, R. Nazikian, A. Alper *et al.*, Phys. Plasmas **13**, 056104 (2006).
[22] M. A. Van Zeeland, G. J. Kramer, R. Nazikian *et al.*, Plasma Phys. Controlled Fusion **47**, L31 (2005).
[23] G. J. Kramer, C. Z. Cheng, Y. Kusama *et al.*, Nucl. Fusion **41**, 1135 (2001).

[24]N. C. Hawkes, B. C. Stratton, T. Tala *et al.*, Phys. Rev. Lett. **87**, 115001 (2001).
[25]W. Kerner, D. Borba, G. T. A. Huysmans *et al.*, Plasma Phys. Controlled Fusion **36**, 911 (1994).
[26]C. Z. Cheng and M. S. Chance, Phys. Fluids **29**, 3695 (1986).
[27]C. T. Holcomb, M. A. Makowski, R. J. Jayakumar *et al.*, Rev. Sci. Instrum. **77**, 10E506 (2006).
[28]W. M. Solomon, K. H. Burrell, P. Gohil *et al.*, Rev. Sci. Instrum. **75**, 3481 (2004); C. Z. Cheng, Phys. Rep. **211**, 1 (1992).
[29]N. N. Gorelenkov, H. L. Berk, and R. V. Budny, Nucl. Fusion **45**, 226 (2005).
[30]R. V. Budny, Nucl. Fusion **42**, 1383 (2002).
[31]S. D. Pinches, V. G. Kiptily, S. E. Sharapov *et al.*, Nucl. Fusion **46**, S904 (2006).
[32]R. B. White, *Theory of Toroidally Confined Plasmas*, 2nd ed. (Imperial College Press, London, 2006).
[33]G. Y. Fu and C. Z. Cheng, Phys. Fluids B **4**, 3722 (1992).
[34]N. N. Gorelenkov and S. E. Sharapov, Phys. Scr. **45**, 163 (1992).